Supporting Information

Single-Component Zero-Dimensional $(BPY)_2ZrCl_6:Sb^{3+}$ Hybrid Perovskite Exhibiting Excitation-Dependent Multi-Color Fluorescence and Afterglow for Advanced Hierarchical Anti-Counterfeiting

Qi Chen [a], Chenyang Zhang [a], Hu Wang [a], Yuexiao Pan [a,], Hongzhou Lian [b], Jun Lin [b,*], Liyi Li [c*]*

[a] *Key Laboratory of Carbon Materials of Zhejiang Province, College of Chemistry and Materials Engineering, Wenzhou University, Wenzhou 325035, P.R. China.*
E-mail: yxpan@wzu.edu.cn

[b] *Key Laboratory of Rare Earth Resource Utilization, Changchun Institute of Applied Chemistry, Chinese Academy of Sciences, Changchun 130022, P. R. China.*
E-mail: jlin@ciac.ac.cn

[c] *Research Center for Eco-environmental Engineering, Dongguan University of Technology, Dongguan, 523808, P. R. China.*
E-mail: liliyi@dgut.edu.cn

1. Experimental section

Materials

N-butyl-pyridinium chloride (BPYCl, Adamas, 99.9%), zirconium (IV) chloride ($ZrCl_4$, Adamas, 99.9%), hydrochloric acid (HCl, 37wt% in water), acetone (C_3H_6O, Adamas, 99.9%), antimony (III) oxide (Sb_2O_3, Adamas, 99.9%). All reagents and solvents were used without further purification and treatment.

Preparation of $(BPY)_2ZrCl_6$ single crystals

A single crystal of $(BPY)_2ZrCl_6$ was successfully synthesized via a conventional hydrothermal synthesis approach. Initially, 0.5 mmol of $ZrCl_4$ and 2.25 mmol of BPYCl were mixed in a 5 mL HCl solution in a 15 mL stainless steel autoclave. Subsequently, the mixture was subjected to thermal treatment at 180 °C for a duration of 12 hours, followed by a controlled cooling to ambient temperature. Then the crystals were washed three times with acetone and dried at 60 °C for 12 hours.

Preparation of $(BPY)_2ZrCl_6$:x%Sb^{3+}

The method similar to that used for synthesizing $(BPY)_2ZrCl_6$ was employed to successfully synthesize $(BPY)_2ZrCl_6$:x%Sb^{3+} (x = 5, 10, 15, 25, 35, and 45) by adjusting different Sb/Zr feed ratios.

Characterization

The crystallographic data for single crystals were obtained using a state-of-the-art SMART APE II DUO X-ray four-circle single crystal diffractometer, equipped with a CCD detector, a graphite monochromator, and a Cu Ka radiation source. Powder X-ray diffraction (XRD) patterns were captured on a Bruker D8 Advance XRD apparatus,

utilizing Cu Ka radiation (l = 0.15418 nm) and scanning at a rate of 5° per minute over a2q range spanning from 5 to 60°. The chemical compositional analysis of the particle surfaces was conducted using Xray photoelectron spectroscopy (XPS) on an ESCALAB 250XiVersaProbe spectrometer, employing Al Ka radiation (hν = 486.6 eV) as the monochromatic X-ray source. The optical properties of the samples were investigated photoluminescence (PL) spectroscopy using a Horiba FluoroMax-4 spectrometer (Horiba, France). The PLQYs measurement was performed using a spectrometer (FLS 980). Thermogravimetric analysis (TGA/SDTA851) of the samples was performed from room temperature to 800 °C at a heating rate of 10 °C min^{-1}. Finally, data processing and graphical plotting were performed using VESTA and Origin software.

Computational methodology

A depiction of the computational framework was utilized in this study, illustrating the application of ab initio simulations grounded in spin-polarized Density Functional Theory (DFT), as implemented in the Vienna Ab initio Simulation Package (VASP).[1] The electronic wave functions were delineated using a plane-wave basis set, with a defined energy cutoff of 350 eV. The Brillouin zone was meticulously sampled with a k-mesh, focusing exclusively on the G point. The unit cell configurations for $(BPY)_2ZrCl_6$ and its Sb^{3+}-doped variants were established with a 3 × 2 × 2 k-point grid, whereas the supercell for Sb^{3+}-doped $(BPY)_2ZrCl_6$ was delineated with a 1 × 1 × 2 k-point grid, accommodating a total of 144 atoms for the comprehensive analysis. For excited-state analysis, time-dependent DFT (TD-DFT) calculations were carried out

using Gaussian 16 to determine the energies of singlet and triplet excited states.[2]

Fabrication of WLEDs devices

The $(BPY)_2ZrCl_6$:5%Sb^{3+} and $(BPY)_2ZrCl_6$:10%Sb^{3+} crystals were ground into fine powders, respectively, and then thoroughly mixed with an A-type epoxy resin and a B-type curing agent at a mass ratio of 1:4 to ensure uniform dispersion of the particles. Subsequently, the resulting mixtures were separately encapsulated onto ultraviolet light-emitting diodes (LEDs) chips with a wavelength of 310 nm and dried at 80 °C for 2 h, thereby obtaining single-component white LEDs.

2. Figures

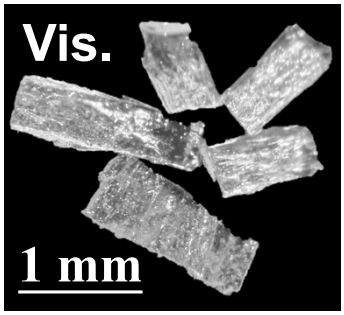

Fig. S1 Photo of pristine $(BPY)_2ZrCl_6$ taken under visible light.

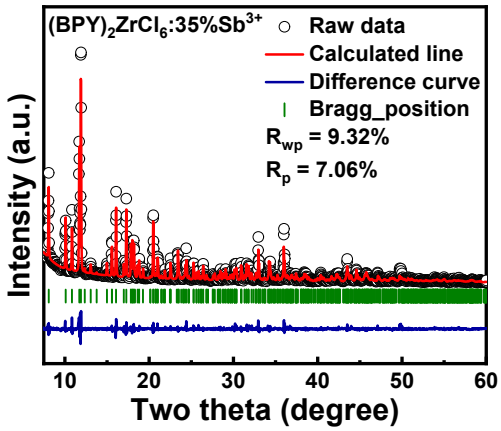

Fig. S2 Rietveld refinement plots of the PXRD patterns and experimental PXRD patterns of $(BPY)_2ZrCl_6$:35%Sb^{3+}.

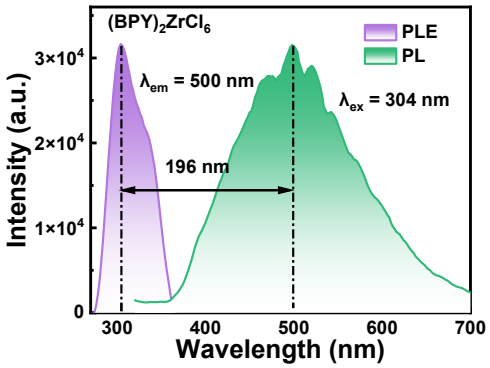

Fig. S3 PLE spectra of $(BPY)_2ZrCl_6$ monitored at 500 nm and PL spectra of $(BPY)_2ZrCl_6$ excited at 304 nm.

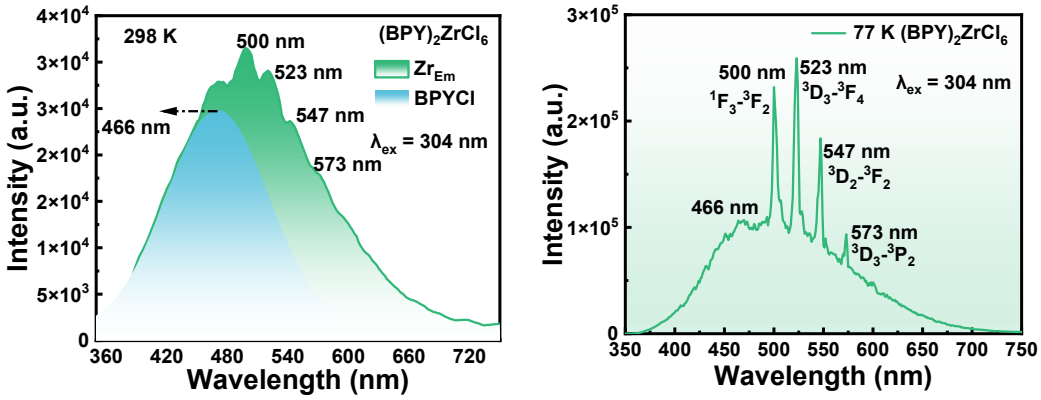

Fig. S4 PL spectra of $(BPY)_2ZrCl_6$ under 304 nm excitation at 298 K and 77 K.

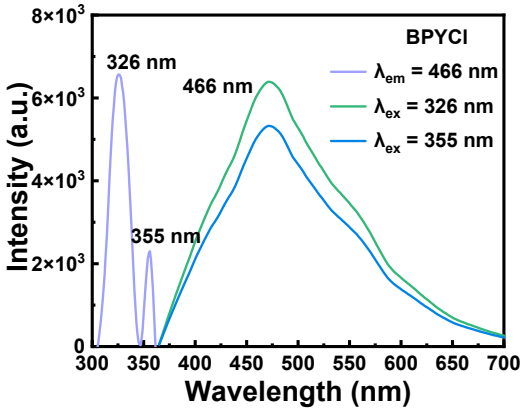

Fig. S5 PLE spectra of BPYCl monitored at 466 nm and PL spectra of BPYCl excited at 326 nm and 355 nm.

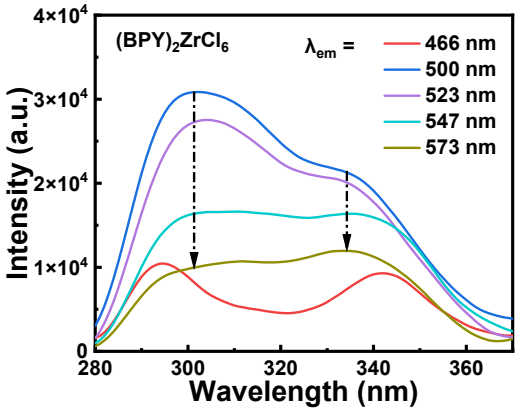

Fig. S6 PLE spectra of $(BPY)_2ZrCl_6$ monitored at 466 nm, 500 nm, 523 nm, 547 nm, and 573 nm.

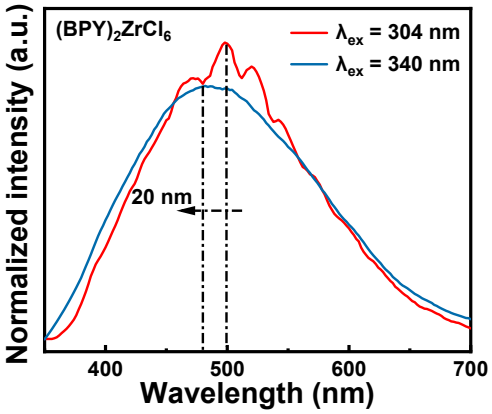

Fig. S7 PL spectra of $(BPY)_2ZrCl_6$ under 304 nm and 340 nm excitation.

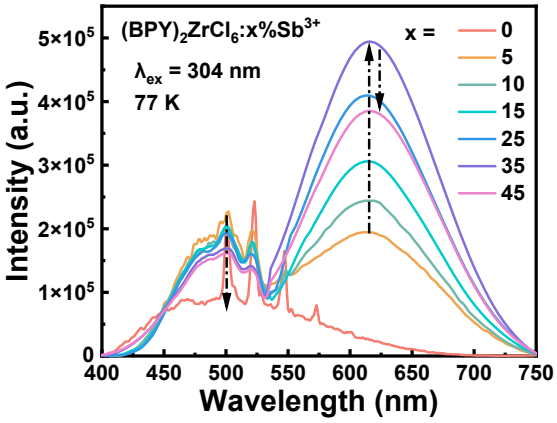

Fig. S8 PL spectra of $(BPY)_2ZrCl_6$:x%Sb^{3+}under 304 nm excitation at 77 K.

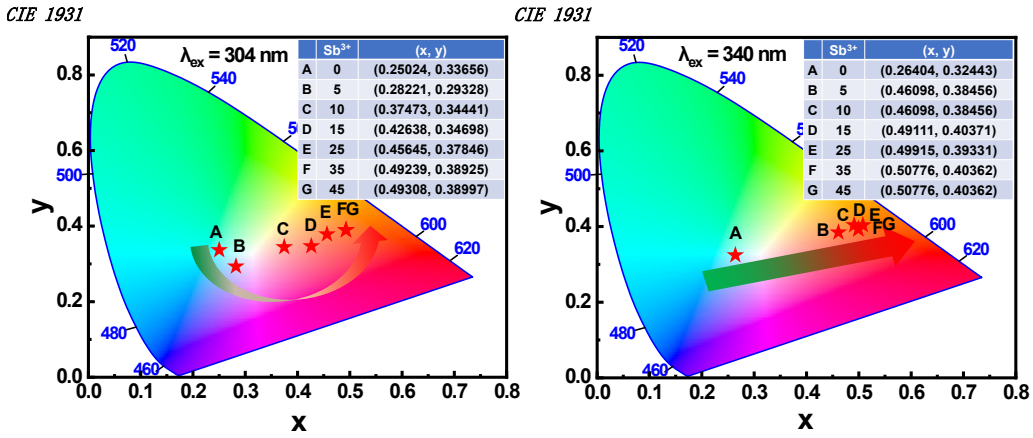

Fig. S9 CIE coordinate of $(BPY)_2ZrCl_6$:x%Sb^{3+} measured at 304 nm and 340 nm.

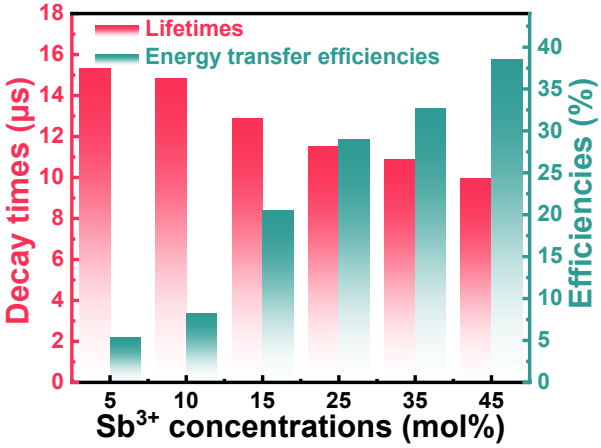

Fig. S10 PL lifetimes and the calculated energy transfer efficiencies with different Sb^{3+} concentrations.

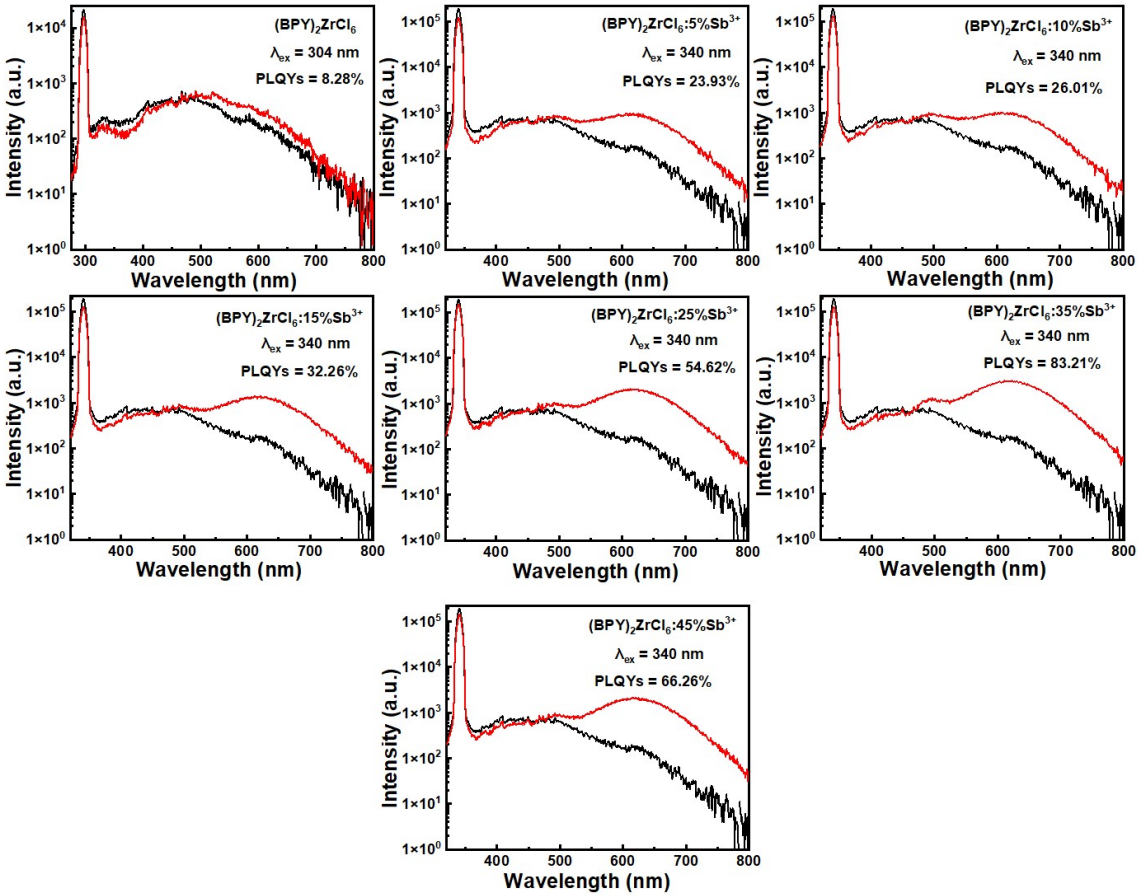

Fig. S11 PLQYs measurement of $(BPY)_2ZrCl_6$:x%Sb^{3+} (x = 0-45) crystals.

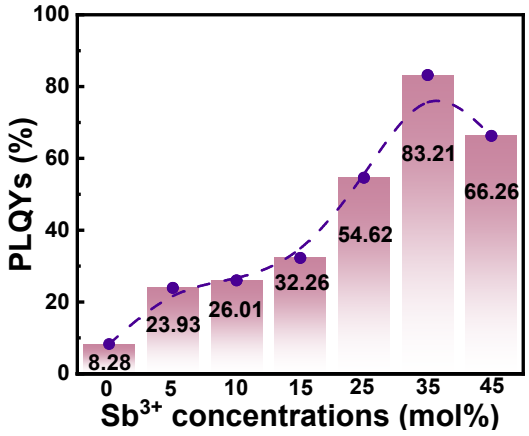

Fig. S12 PLQYs of $(BPY)_2ZrCl_6$:x%Sb^{3+}.

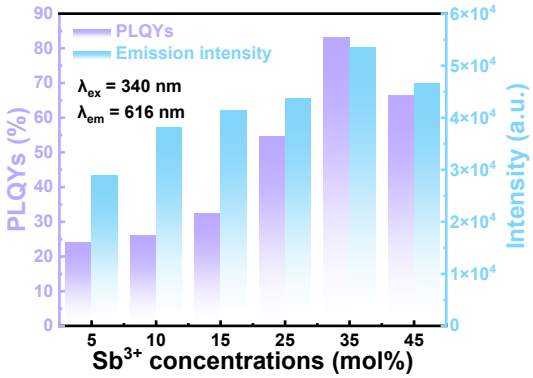

Fig. S13 PLQYs and emission intensity of $(BPY)_2ZrCl_6$:x%Sb^{3+} varied with the concentration of Sb^{3+}.

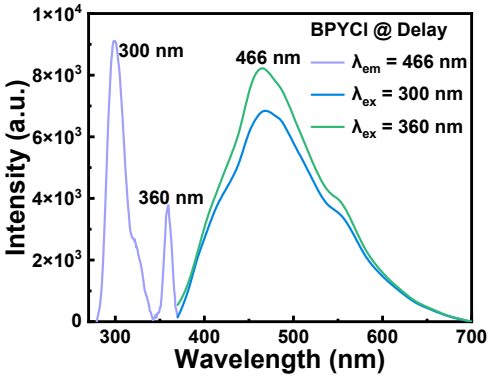

Fig. S14 Delayed PLE spectra of BPYCl monitored at 466 nm and delayed PL spectra of BPYCl excited at 300 nm and 360 nm.

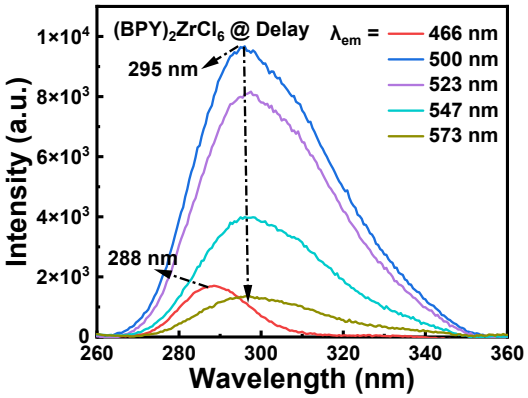

Fig. S15 Delayed PLE spectra of $(BPY)_2ZrCl_6$ monitored at 466 nm, 500 nm, 523 nm, 547 nm, and 573 nm.

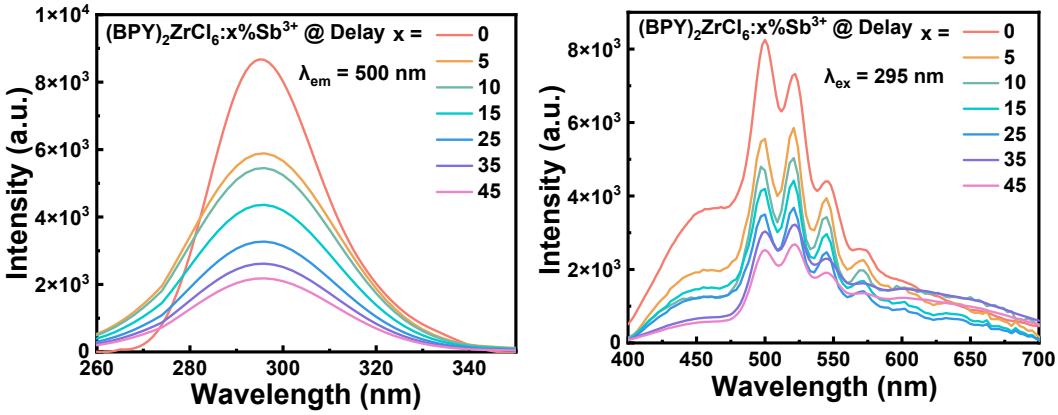

Fig. S16 Delayed PLE/PL spectra of $(BPY)_2ZrCl_6$:x%Sb^{3+} (x = 0-45).

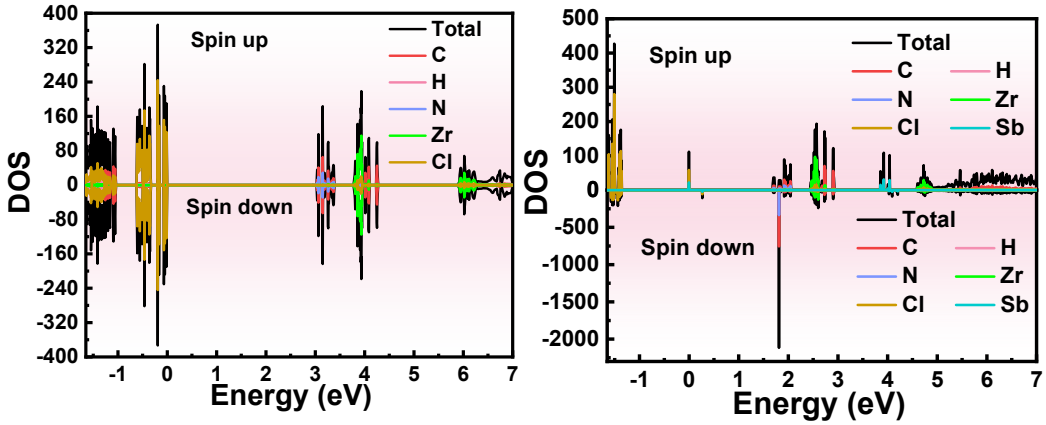

Fig. S17 Band structure with spin-polarization of $(BPY)_2ZrCl_6$ and $(BPY)_2ZrCl_6$:Sb^{3+}.

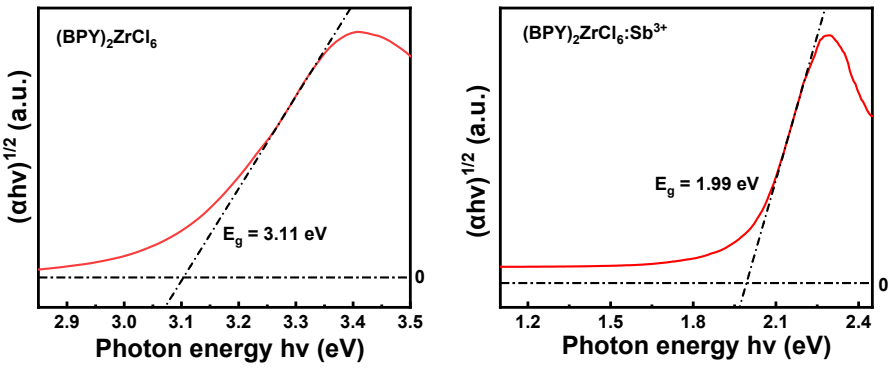

Fig. S18 Graphs of the relationship between $(BPY)_2ZrCl_6$ and $(BPY)_2ZrCl_6:Sb^{3+}$ crystal $(\alpha hv)^{1/2}$ and photon energy.

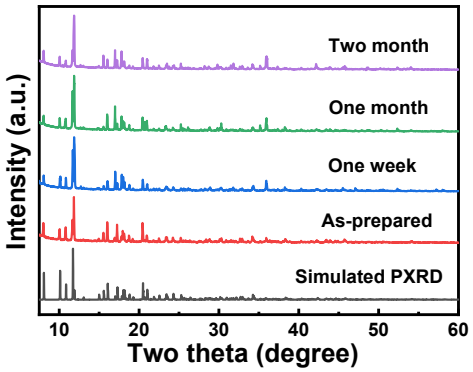

Fig. S19 PXRD of $(BPY)_2ZrCl_6:35\%Sb^{3+}$ after being exposed to air for different periods of time.

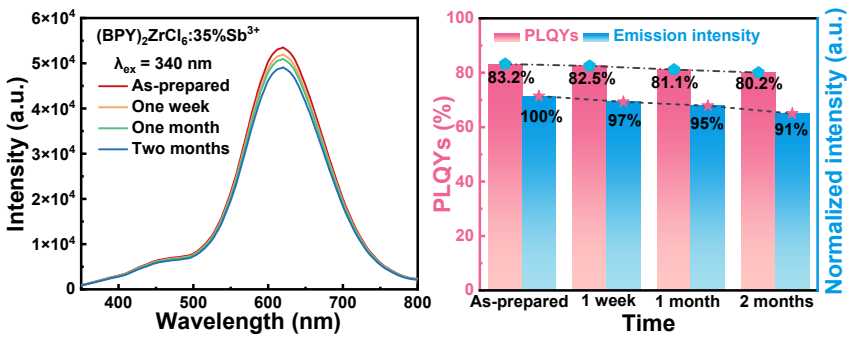

Fig. S20 PL spectra of $(BPY)_2ZrCl_6:35\%Sb^{3+}$ after being exposed to air for different periods of time, PLQYs and emission intensity of $(BPY)_2ZrCl_6:35\%Sb^{3+}$ after being exposed to air for different periods of time.

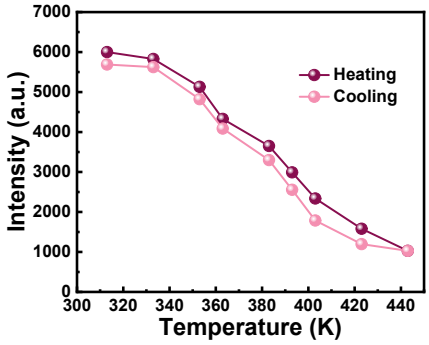

Fig. S21 PL intensity of $(BPY)_2ZrCl_6$:35%Sb^{3+} as a function of measurement temperature in the range of 313-443 K.

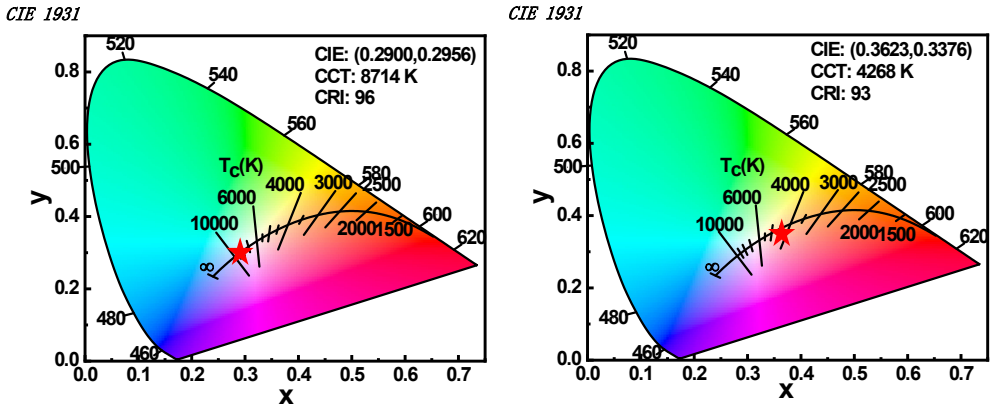

Fig. S22 The CIE coordinates of the WLEDs constructed using $(BPY)_2ZrCl_6$:x%Sb^{3+} (x = 5, 10) materials on a 310 nm ultraviolet chips.

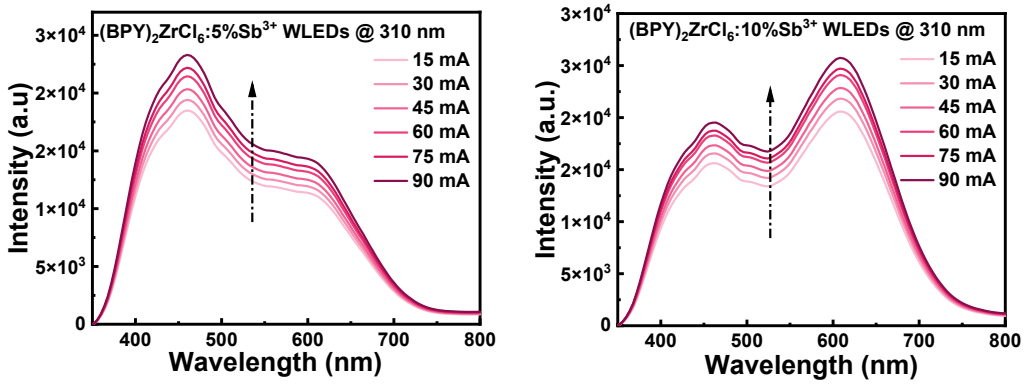

Fig. S23 EL spectra of $(BPY)_2ZrCl_6$:x%Sb^{3+} (x = 5, 10)-based WLEDs under different applied current.

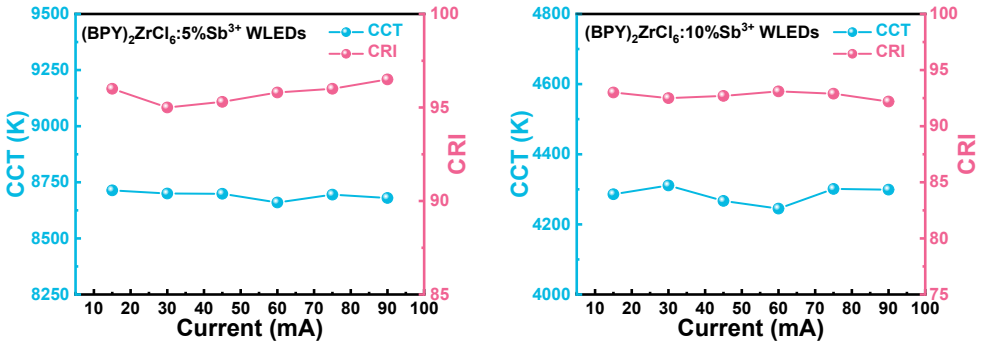

Fig. S24 CCT, CRI of $(BPY)_2ZrCl_6$:x%Sb^{3+} (x = 5, 10)-based WLEDs under different applied current.

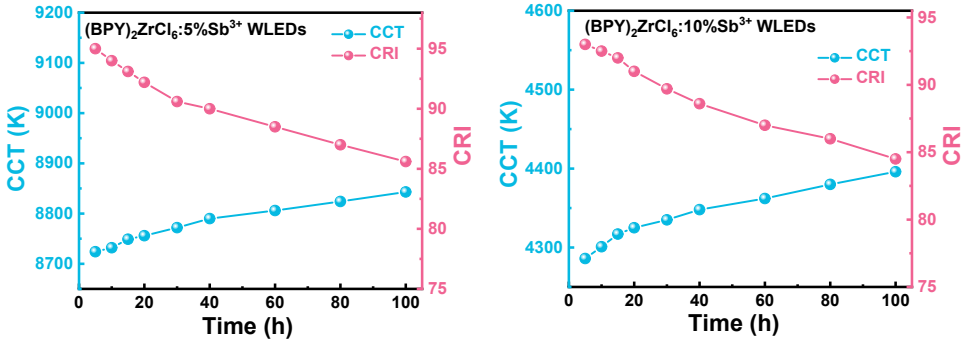

Fig. S25 CCT, CRI of $(BPY)_2ZrCl_6$:x%Sb^{3+}(x = 5, 10)-based WLEDs over 100 hours of continuous operation.

3. Tables

Table S1. Crystal data and structure refinement for $(BPY)_2ZrCl_6$.

Empirical formula	**$C_{18}H_{28}Cl_6N_2Zr$**
Formula weight	576.34
Temperature/K	296.1 (3)
Crystal system	monoclinic
Space group	$P2_1/c$
***a*/Å**	15.0154 (7)
***b*/Å**	16.4714 (6)
***c*/Å**	10.4913 (5)
***α*/°**	90
***β*/°**	90.020 (4)
***γ*/°**	90
Volume/Å^3	2594.8 (2)
Z	4
ρ_{calc}g/cm^3	1.470
μ/mm^{-1}	1.048
***F* (000)**	1160.0
Crystal size/mm^3	0.4 × 0.3 × 0.2
Radiation	Mo Kα (λ = 0.71073)
2Θ range for data collection/°	4.604 to 60.024
Index ranges	$-18 \leq h \leq 19$, $-19 \leq k \leq 22$, $-13 \leq l \leq 11$
Reflections collected	16316
Independent reflections	5832 [R_{int} = 0.0221, R_{sigma} = 0.0263]
Data/restraints/parameters	5832/8/246
Goodness-of-fit on F^2	1.048
Final R indexes [I>=2σ (I)]	R_1 = 0.0385, wR_2 = 0.0959
Final R indexes [all data]	R_1 = 0.0585, wR_2 = 0.1055
Largest diff. peak/hole / e Å^{-3}	0.41/-0.35

Table S2. Lattice parameters a, b, and c axes of the Rietveld refinement of $(BPY)_2ZrCl_6$:x% Sb^{3+}.

$(BPY)_2ZrCl_6$:x%Sb^{3+}	**a (Å)**	**b (Å)**	**c (Å)**
0	15.01540	16.47140	10.49130
5	15.00758	16.48529	10.49548
10	15.00905	16.49520	10.50055
15	15.01546	16.49368	10.50102
25	15.00653	16.49821	10.50213
35	15.02407	16.50163	10.50453
45	15.02608	16.49216	10.50941

4. References

1 G. Kresse, and J. Hafner, *Ab Initio* Molecular Dynamics for Liquid Metals, *Phys. Rev. B*. 1993, **47**, 558.

2 M. J. Frisch, G. W. Trucks, H. B. Schlegel, G. E. Scuseria, M. A. Robb, J. R. Cheeseman, G. Scalmani, V. Barone, G. A. Petersson, H. Nakatsuji, X. Li, M. Caricato, A. V. Marenich, J. Bloino, B. G. Janesko, R. Gomperts, B. Mennucci, H. P. Hratchian, J. V. Ortiz, A. F. Izmaylov, J. L. Sonnenberg, D. Williams-Young, F. Ding, F. Lipparini, F. Egidi, J. Goings, B. Peng, A. Petrone, T. Henderson, and D. Ranasinghe, Gaussian 16, Revision B.01, Gaussian Inc, Wallingford, CT 2016.